ICASE

NUMERICAL COMPUTATIONS OF TURBULENCE AMPLIFICATION IN SHOCK WAVE INTERACTIONS

Thomas A. Zang
M. Y. Hussaini
Dennis M. Bushnell

Report No. 83-10

April 28, 1983

INSTITUTE FOR COMPUTER APPLICATIONS IN SCIENCE AND ENGINEERING
NASA Langley Research Center, Hampton, Virginia 23665

Operated by the

UNIVERSITIES SPACE USRA RESEARCH ASSOCIATION

NUMERICAL COMPUTATIONS OF TURBULENCE AMPLIFICATION IN SHOCK WAVE INTERACTIONS

Thomas A. Zang*
College of William and Mary

M. Y. Hussaini**
Institute for Computer Applications in Science and Engineering

Dennis M. Bushnell†
NASA Langley Research Center

Abstract

Numerical computations are presented which illustrate and test various effects pertinent to the amplification and generation of turbulence in shock wave-turbulent boundary layer interactions. Several fundamental physical mechanisms are identified. Idealizations of these processes are examined by nonlinear numerical calculations. The results enable some limits to be placed on the range of validity of existing linear theories.

---

*Research Associate, supported by NASA Grant NAG1-109.

**Senior Staff Scientist, ICASE, NASA Langley Research Center, Hampton, VA, supported by the National Aeronautics and Space Administration under NASA Contract Nos. NAS1-15810, NAS1-16394, and NAS1-17070.

†Head, Viscous Flow Branch, High-Speed Aerodynamics Division, NASA Langley Research Center, Associate Fellow AIAA.

Introduction

The application of low-speed turbulence modeling approaches to the calculation of high-speed boundary layers has proven quite successful, even up to Mach numbers on the order of 20 (e.g., Ref. 1). However, for shock wave-turbulent boundary layer interactions computational results which are based on essentially low-speed turbulence models are generally unsatisfactory when applied to separated flow cases, where the mean flow is no longer largely pressure driven (e.g., Refs. 2-3). The shock wave, from a simplistic viewpoint, could be considered as a very steep pressure gradient. Indeed, low-speed information, both theoretical and experimental (e.g., Refs. 4-5), for such pressure gradients indicate that "rapid distortion" concepts hold and, in the limit of extremely sharp gradients the Reynolds stress and turbulence intensities are "frozen," since there is insufficient residence time in the gradient for the turbulence to alter at all, let alone equilibrate. However, experimental information for shock wave-boundary layer interactions indicates significant amplifications of Reynolds stress and turbulence intensity across the shock wave (e.g., Refs. 6-11) and subsequent improvement in the capacity to withstand separation (Ref. 12). Evidently some new physics, associated perhaps with compressibility phenomena, is responsible for this amplification. This is a situation where our extraordinary good fortune in applying low-speed turbulence modeling to high-speed flows has expired.

The simpler aspects of the shock wave-turbulence interaction, i.e., the basically linear effects, are amenable to analysis. The decomposition of a general fluctuation into acoustic, entropy, and vorticity waves is well-known (e.g., Ref. 13). Some three decades ago, Moore (Ref. 14), Ribner (Ref. 15), Chang (Ref. 16), and Kerrebrock (Ref. 17), examined the effects of a shock

upon various linear plane waves (see also Refs. 18-22). In general, whenever any of these waves passes through a shock, it will generate the other two waves downstream in addition to itself undergoing transmission and refraction. The transmission and generation coefficients for this process were a primary product of the work cited above.

The principal application of these results has been to the noise produced downstream of the shock. Recently, Anyiwo and Bushnell (Ref. 23) used the analytical results to reassess the amplification and generation of turbulence in shock wave interactions. Their results combined with the experimental data on shock wave-boundary layer interactions lead the present authors to suggest that there are at least four mechanisms which are responsible for turbulence enhancement across a shock wave, viz:

1. Amplification of incident turbulence (vorticity fluctuations) across a shock wave.
2. Generation of turbulence behind a shock wave due to incident acoustic or entropy fluctuations.
3. Unsteady focusing of high frequency vorticity behind the shock wave due to shock distortions caused by low frequency fluctuations.
4. Direct conversion of mean flow energy into turbulence by shock oscillation.

The significance of the first two mechanisms is clear. Moreover, in a shocked region several shock and compression wave surfaces are usually present, across and on which refraction, reflection, generation, and re-reflection of fluctuation modes may easily create acoustic, turbulence, and entropy fluctuations far in excess of the values incident upon the shocked region. Thus, mechanisms 1 and 2 together can represent a very significant turbulence amplifier in compressible boundary layer-shock interaction problems (Ref. 23).

Focusing effects leading to high intensity, localized turbulence have been consistently observed in the propagation of sonic booms through atmospheric turbulence (Ref. 24) and Ref. 25 indicates that this mechanism may be especially significant in the transonic regime. Shock oscillations, both translational and rotational, are prominent in shock wave-boundary layer experiments (Refs. 26 and 27) and are particularly virulent in the separated flow case (Ref. 28). This, of course, is where the greatest difficulty in turbulence modeling is encountered. The genesis of these oscillations is thought to be a combination of large-scale "breathing" (low frequency instability) of the separated flow and shock reflection from a sonic "line" which distorts in space-time due to turbulent flow fluctuations.

The actual physical problem of shock wave-turbulent boundary layer interaction is (especially for transonic flow facilities) further complicated by the presence of incoming pressure disturbances from the free stream (Ref. 29) and by details of the quasi-inviscid wave field (Ref. 30).

The purpose of the present investigation is to investigate numerically, using the full nonlinear two-dimensional Euler equations, some of the various turbulence enhancement mechanisms enumerated above. The numerical computations to be presented here address mechanisms 1 and 2. Detailed comparisons are made between the linear, plane wave predictions and the nonlinear results. At low amplitudes the analytic results provide a check on the numerical procedures. At high amplitudes the nonlinear results remain valid and offer practical limits to the linear theory. In a subsequent paper numerical calculations for coherent structures relevant to the first two mechanisms will be presented along with the calculations pertaining to mechanisms 3 and 4.

Numerical Method

The shock wave-turbulent boundary layer interaction is sufficiently complex that it is effectively impossible to isolate experimentally its basic physical mechanisms. Numerical computations offer a means to examine individual effects under controlled conditions. However, not even two-dimensional direct Navier-Stokes simulations of the shock wave-turbulent boundary layer problem are yet feasible. The compromise that will be adopted here is to perform numerical computations of a simpler situation: interactions of turbulence with shock waves in an ideal fluid. The neglect of viscous effects does not appear too serious, for the principal issue is how turbulence is amplified by passage through the shock. The analysis given in Ref. 13 provides a means to estimate the significance of viscous effects. The numerical computations do include the potentially crucial compressible and nonlinear effects.

Model Problem

The model problem which is used to study the turbulence amplification and generation mechanisms is illustrated in Figure 1. At time $t = 0$ an infinite, normal shock at $x = 0$ separates a rapidly moving, uniform fluid on the left from the fluid on the right which is in a quiescent state except for some specified fluctuation. The initial conditions are chosen so that in the absence of any fluctuation the shock moves uniformly in the positive x-direction with a Mach number (relative to the fluid on the right) denoted by M_s. In the presence of fluctuations the shock front will develop ripples. The structure of the shock is described by the function $x_s(y,t)$. The numerical calculations are used to determine the state of the fluid in the region between the shock front and some suitable left boundary $x_L(t)$ and also to determine the motion and shape of the shock front itself.

Governing Equations

The physical domain in which the fluid motion is computed is given by

$$\begin{aligned} x_L(t) &\leq x \leq x_s(t) \\ -\infty &< y < - \\ t &\geq 0. \end{aligned} \tag{1}$$

The change of variables

$$X = \frac{x - x_L(t)}{x_s(y,t) - x_L(t)}$$

$$Y = \frac{1}{2}\left[1 + \tanh(\alpha y)\right] \tag{2}$$

$$T = t,$$

produces the computational domain

$$\begin{aligned} 0 &\leq X \leq 1 \\ 0 &\leq Y \leq 1 \\ T &\geq 0. \end{aligned} \tag{3}$$

The stretching parameter α is typically of order 1.

The fluid motion is presumed to be governed by the two-dimensional Euler equations. In terms of the computational coordinates these are

$$Q_T + B\,Q_X + C\,Q_Y = 0, \tag{4}$$

where

$$Q = [P,u,v,S], \tag{5}$$

$$B = \begin{bmatrix} U & \gamma X_x & X_y & 0 \\ \frac{c^2}{\gamma} X_x & U & 0 & 0 \\ \frac{c^2}{\gamma} X_y & 0 & U & 0 \\ 0 & 0 & 0 & U \end{bmatrix}, \tag{6}$$

and

$$C = \begin{bmatrix} V & \gamma Y_x & \gamma Y_y & 0 \\ \frac{c^2}{\gamma} Y_x & V & 0 & 0 \\ \frac{c^2}{\gamma} Y_y & 0 & V & 0 \\ 0 & 0 & 0 & V \end{bmatrix}. \tag{7}$$

The contravariant velocity components are given by

$$U = X_t + uX_x + vX_y$$

and (8)

$$V = Y_t + uY_x + vY_y.$$

A subscript denotes partial differentiation with respect to the indicated variable. P, c, and S are the natural logarithm of pressure, the sound speed, and the entropy (divided by the specific heat at constant volume), respectively, all normalized by reference conditions at downstream infinity; u and v are velocity components in the x- and y-directions, both scaled by the characteristic velocity defined by the square root of the pressure-density ratio at downstream infinity. The ratio of specific heats is denoted by γ; a value $\gamma = 1.4$ has been used for all the calculations in this paper. The magnitude of the velocity will be denoted by w.

Discretization

This equation set is discretized using the well-known finite difference method of MacCormack (Ref. 31). This is a two-step, explicit, second-order accurate method of Lax-Wendroff type. The finite difference grid in the computational plane is fixed and uniform. Since the shock front moves to the right in the course of the calculation, the corresponding discrete grid in the physical plane is expanding. Thus, the effective resolution in the x-direction continually decreases during the evolution. Eventually the resolution of any calculation will become inadequate and the results will no longer be reliable. Fortunately, in many situations the important information can be extracted before this occurs, especially if the initial grid is taken to be an exceedingly fine one.

The most delicate part of the calculation is the treatment of the shock front. A shock-fitting approach is used here because it avoids the severe oscillations that can accompany shock-capturing methods. Briefly put, an appropriate time derivative of the Rankine-Hugoniot relations provides an equation for the shock acceleration. This equation is integrated to update the shock position. The formula for the shock acceleration is a generalization of the one used by Pao and Salas (Ref. 32) in their numerical study of the shock-vortex interaction. The difference is that the present application requires allowances to be made for a time-dependent flow ahead of the shock. A detailed description of this part of the algorithm will be available in Ref. 33.

The right boundary at $x_s(y,t)$ is a supersonic inflow boundary. Hence it is appropriate to prescribe all variables there. The correct boundary conditions at the left boundary at $x_L(t)$ depend upon the relative shock Mach number. If $M_s > 2.08$, then the flow behind the shock is supersonic. In this

case the left boundary is again a supersonic inflow boundary and it is appropriate to prescribe all variables there. If $M_s < 2.08$, then the left boundary is a subsonic inflow boundary. The simplest procedure is to stop the calculations before the time at which disturbances first reach the left boundary. At the top and bottom boundaries (which have been stretched to infinity in the physical plane) zero disturbance boundary conditions are enforced. This is certainly justifiable whenever the fluctuations decay rapidly in these directions. However, there will be spurious reflections from the upper and lower boundaries if the disturbances extend that far out. The spurious reflections that will emanate from these boundaries need not pose a serious problem since the decreasing resolution resulting from the shock motion already limits the useful duration of a calculation. More sophisticated boundary conditions are discussed in Ref. 33.

Interaction of Plane Waves with Shocks

Summary of Linear Theory

Perhaps the simplest formulation of the linear theory of the interaction of plane waves with a shock is due to McKenzie and Westphal (Ref. 44). This work, referred to below as MW, was performed very much later than the pioneering studies cited in the introduction. But since it leads to equivalent results and is more accessible and tractable than the others it will be used as the basis for comparing the nonlinear calculations with the analytical predictions.

A standard setting for the two-dimensional linear theory is depicted in Fig. 2. A uniform, supersonic flow undergoes a shock and emerges as subsonic. Flow quantities ahead of the shock (on the right) are denoted by a

subscript 1 and those behind by a subscript 2. In each region of uniform flow the linearized Euler equations admit plane waves of the form

$$A' e^{i(\underline{k}\cdot\underline{x}-\omega t)}, \tag{9}$$

where A' is the wave amplitude, $\underline{k}$ is the wavevector, and ω the frequency. The three distinct types of linear waves and their basic properties are given in Table 1. The normalized amplitude of each wave type is denoted by A' with an identifying subscript. Since the mean flow is to the left, the fast acoustic wave uses the negative sign in the dispersion relation. A slow acoustic wave can also be present under some circumstances.

Table 1. Properties of Linear Waves

Wave Type	Components	Dispersion Relation
Acoustic	$p' = A'_p$ $\underline{u}' = (k_x,k_y)(1/\rho ck)A'_p$ $S' = 0$	$\omega = \underline{u}\cdot\underline{k} - kc$
Vorticity	$p' = 0$ $\underline{u}' = (-k_y,k_x)(c/pk)A'_v$ $S' = 0$	$\omega = \underline{u}\cdot\underline{k}$
Entropy	$p' = -(\rho/p)A'_e$ $\underline{u}' = (0,0)$ $S' = (\gamma/p)A'_e$	$\omega = \underline{u}\cdot\underline{k}$

The only coupling that exists between these linear waves occurs at the shock front. It is this coupling that is responsible for the situation displayed in the figure: an incident fast acoustic wave whose wave front is inclined at an angle θ_1 to the shock front produces a transmitted fast acoustic wave at an angle θ_2 and generates both an entropy and a vorticity wave at an angle θ_3. The analytic nature of the wave coupling occurs in the boundary conditions applied at the shock. They are applied not at the distorted shock surface itself but rather at the undisturbed shock front. As the actual shock distortion increases, the linearized boundary conditions become less reliable.

The key results of the linear theory are the transmission and generation coefficients. For an incident vorticity wave

$$A'_{v,2}/A'_{v,1} = (p_2/c_2)\, w'_2/(p_1/c_1)w'_1$$

$$A'_{p,2}/A'_{v,1} = p'_2/(p_1/c_1)w'_1 \qquad (10)$$

$$A'_{e,2}/A'_{v,1} = (\gamma/p_2)\, S'_2/(p_1/c_1)w'_1$$

are, respectively, the transmission coefficient for the vorticity wave, the generation coefficient for the acoustic wave and the generation coefficient for the entropy wave. The symbol w' denotes the magnitude of a fluctuating velocity associated with a vorticity wave. The transmission coefficient for incident acoustic and entropy waves are defined in an analogous manner. The scaling used in defining these coefficients is the one adopted in Ref. 34. These "MW units" are convenient for the comparison between linear and nonlinear results, but they disguise the magnitude of the velocity

fluctuations, which are the quantities of most interest for turbulence. Table 2 provides some conversion factors which are useful for translating the data presented in the following sections into suitably-scaled velocity fluctuations.

Table 2. Conversion Factor for the MW Units

Mach Number	$\left(\frac{w_1'}{u_1}\right)\Big/A_{v,1}'$	$\left(\frac{w_2'}{u_2}\right)\Big/A_{v,2}'$	$\left(\frac{w_2'}{u_2} / \frac{w_1'}{u_1}\right)\Big/(A_{v,2}'/A_{v,1}')$
1.1	0.909	0.881	0.969
1.5	0.667	0.580	0.870
2.0	0.500	0.385	0.770
8.0	0.125	0.034	0.273

The formulas for these coefficients are available in Ref. 34. The essential equations there are numbers (3), (9), (10), (22) through (25), (30), (35), and (39). Equation (24) contains a typographical error: the first occurrence of M_{1n}^2 in the numerator should be replaced by $M_{1n}^2 \alpha_{1n}^2$. The interested reader is advised against using any equation other than those listed above without first checking it for himself since the remaining equations in Ref. 34 contain numerous typographical errors. Reference 23 contains a summary of the mathematical details phrased in terms customary to analyses of turbulence.

For sufficiently high angles of incidence for the wave ahead of the shock, the acoustic wavevector $\underline{k}_2$ has a nonzero imaginary part. Under such

circumstances the acoustic response is not an infinite plane wave; instead, it exhibits an exponential decay in the x-direction behind the shock. The incidence angle that separates the plane wave acoustic responses from the decaying ones is called the critical angle. Linear theory predicts that most transmission and generation coefficients are peaked near the critical angle.

Numerical Simulation

The numerical simulation of plane waves differs slightly from the idealized, steady-state situation treated by linear theory. In the linear theory the coordinate system is usually chosen so that the shock is stationary. For computational purposes it is more convenient to have the shock moving to the right into a region of stationary mean flow downstream. The calculations are posed as an initial-value-problem and are performed on a domain which is finite in the x-direction.

At the initial instant $t = 0$ all the fluid in the computational domain, which extends from the left boundary (typically at $x = -0.5$) to the shock location at $x = 0$, is in uniform flow. The fluid is immediately affected by the downstream plane wave through the inflow conditions applied at the shock. As the calculation proceeds the effects of the incident wave spread into an increasing portion of the fluid behind the shock.

The specific inflow conditions are obtained by superimposing one of the perturbations listed in Table 1 (after a Galilean transformation into the computational frame) onto the downstream mean flow. The wave type, amplitude A', angle of incidence θ_1, and wavenumber k must be specified. Since the calculations are performed in units such that the downstream pressure $p_1 = 1$, an incident acoustic wave with amplitude $A' = 0.01$ corresponds to a maximum downstream pressure perturbation of 1%.

Figure 3 displays several stages of a calculation for which a Mach 8 shock encounters a 1% vorticity wave with wavenumber $k = 2\pi$ and inclined at 30° to the shock. At the initial instant (shown in the first column) the fluid behind the shock is in uniform flow and the flow downstream consists of a pure shear wave. The second and third columns of Fig. 3 indicate the computational results at two subsequent times. There is a noticeable departure from the plane wave shape at the leading edges of the post-shock waves. This is to be expected given the suddenness with which the downstream perturbation is encountered. Note that the velocity vectors well behind the shock are indicative of a pure acoustic wave, whereas those closer to the shock display some vorticity.

In this sort of diagram the downstream flow is given for illustrative purposes only — it is not part of the actual calculations. Moreover, the results have been interpolated from the nonuniform grid used in the computations to a uniform grid in the physical domain suitable for plotting. Since the vorticity results require both an interpolation and a numerical differentiation, this portion of the results is intrinsically less reliable than the remainder. The velocity vectors behind the shock represent perturbations from the mean flow. They are drawn to the same scale as the velocities in the downstream region. However, different scales are used at each time. The contour levels are uniformly spaced so that 10 levels are plotted between the minimum and maximum values. Thus, the contour scales also differ at each instant. The drastic amplification that occurs in most high Mach number cases renders a uniform contour scale undesirable. A 75×50 grid was used in the computations for Fig. 3. The plotting domain extends from -0.5 to 2.5 in x and from -1.0 to 1.0 in y. There are a dozen computational points with $|y| > 1$. For sufficiently large $|y|$ the

computational grid can no longer resolve the y-dependence of the wave. No spurious reflections were yet in evidence when this calculation was stopped.

The computational results are clearly in qualitative agreement with the linear theory predictions. The principal aim of this study is to make a quantitative comparison. To do this, it is necessary to estimate wave amplitudes in the upstream region. The first step taken here was to transfer the quantity of interest, e.g., pressure, from the computational grid onto a grid which is uniform in the physical coordinates x and y. Quadratic interpolation was used in this procedure. Next, for each value of x a least squares fit to a function of the form

$$a_0 + a_c \cos(k_y y) + a_s \sin(k_y y) \tag{11}$$

was performed. The wave amplitude at that value of x was taken to be the quantity $\sqrt{a_c^2 + a_s^2}$. These amplitudes can then be averaged over an appropriate range in x to obtain a single numerical estimate of a transmission or generation coefficient. Samples of the x-dependent amplitudes are given in Fig. 4.

Although the actual transmission/generation coefficients are independent of the incident wavelength $\lambda = 2\pi/k$ in the linear limit, the quality of a numerical simulation depends upon this parameter. There are two competing considerations. As λ increases, the number of grid points per wavelength increases. This leads to better numerical resolution. However, as λ decreases the shock passes over more waves during a given time interval. This leads to a more rapid attainment of the steady responses. Since the numerical grid coarsens as the calculation proceeds, some compromise between these two demands is necessary. Our experience has been that reliable simulations

require that at least one full wavelength be established upstream of the shock and that there be at least 10 points per wavelength at the end of the calculation.

Results for Strong Shocks

The regimes for which the assumptions of linear theory appear suspect are weak shocks, strong disturbances, and the vicinity of the critical angles. Mach 8, with a pressure ratio of 74.5, provides an example of a strong shock. The critical angles are roughly 73.8° for incident acoustic waves and 67.2° for incident entropy and vorticity waves. Thus there is adequate representation of both the plane wave response region and the exponentially-damped response region. Moreover, the many linear results for Mach 8 given in Ref. 34 furnish a ready check on the present procedures.

Nonlinear results for the transmission/generation coefficients are given as a function of the angle of incidence and compared with linear theory in Fig. 5. A negative coefficient indicates a phase change. The linear predictions are not shown beyond the critical angle. A 75×50 grid and a wavelength $\lambda = 2$ were used for the calculations presented in this figure. A single data point (along with the standard deviation denoted by the error bars) was obtained by averaging the x-dependent response values, such as those illustrated in Fig. 4, over most of the region in which the disturbance exists. The error bars have been suppressed whenever they fall within the symbol.

The linear predictions agree well with the simulation results at low angles of incidence but they disagree sharply at the larger angles. The discrepancy sets in at about 50° for the acoustic responses and only near the critical angles for the vorticity responses. Linear theory predicts that the

pressure responses change abruptly from constant amplitude plane waves to exponentially-decaying ones at the critical angles. The simulations do not display this behavior. Exponentially-decaying amplitudes appear in the acoustic responses well before the critical angle is reached. Figure 6 gives one example. This accounts for the absence of any acoustic response data beyond 60°. The vorticity responses remain constant-amplitude plane waves beyond the critical angle. However, they do not exhibit the linear prediction of an abrupt change of phase (for generated vorticity) or an abrupt increase in magnitude (for transferred vorticity) near the critical angle. Many additional calculations have been performed to verify this result of the nonlinear simulations. The responses were calculated for 1° increments in the angle of incidence near the critical angles. Computations were performed on coarser meshes, with both larger and smaller incident wavelengths, at different amplitudes, and for slightly longer durations. We have even performed the calculations with a pseudospectral rather than a finite difference spatial discretization (Ref. 35). Results within the error bars have consistently been obtained. A similar discrepancy at large angles of incidence also appears in the entropy responses.

On the other hand, the linear theory has proven quite robust at the smaller angles of incidence. Figure 5 indicates that there is no significant difference in the transmission/generation coefficients between 0.1% and 10% incident amplitude. (The one apparent exception — the 10° acoustic transfer coefficient — is probably caused by the ill-conditioning of the least squares fit at low incidence angles.) Calculations at higher amplitudes for 30° waves suggests that linear theory is valid for acoustic wave amplitudes up to 25% and for vorticity wave amplitudes up to 100%. In the latter case the upstream velocity fluctuations are 73% of the mean stream.

Results for Weak Shocks

Since the shock weakens as the Mach number tends to 1, the shock front will undergo greater distortions from an incident wave of fixed amplitude. Thus, nonlinear effects ought to be increasingly important for lower Mach numbers. The second set of response calculations deals with Mach numbers in the range between 1 and 2. Waves incident at an angle of 30° to the shock have been singled out for these calculations. Both critical angles are much larger than this — close to 90° for incident acoustic waves and roughly 60° for incident entropy or vorticity waves.

The computational results are displayed in Figs. 7, 8, and 9 as functions of the Mach number and of the amplitude. In each case the transmission coefficient is displayed on top and one of the generation coefficients on bottom. The vorticity response is always shown because of its interest for the turbulence amplification question.

For all three types of waves the agreement between the predicted and the computed transmission coefficients is remarkable. This holds both for very low Mach numbers and for sizeable amplitudes. The limiting effect appears to be the nonlinear dynamics in the upstream region. At an appropriate combination of low Mach number and high incident wave amplitude the refracted acoustic wave steepens into a secondary shock parallel to its wave front.

All the results given in Figs. 7 to 9 are consistent in the sense that both the generation and transmission coefficients for a given case were extracted from the same calculation. An alternative strategy would have been to take these coefficients from separate runs in which the best incident wavelength was used for each coefficient. But this would not have permitted us to assess any nonlinear effects that might arise because of wave interactions at appreciable amplitudes. The major conclusion that we can draw

about the regions of validity of linear theory is that it is quite broad. It extends to very low (but still supersonic) Mach numbers and to substantial amplitudes.

In most cases the generation coefficients also agree with the linear theory. The most significant disagreement occurs for the Mach 2 acoustic responses to vorticity waves. The results shown in Fig. 7 were obtained with an incident wavelength $\lambda = 2$. For $\lambda = 1$ the acoustic responses agree much better but the vorticity responses are not as good. This trade-off is also present to a lesser extent in the other calculations for low Mach numbers - vorticity responses benefit from a longer incident wavelength and acoustic responses from a shorter one. For a 30° incident vorticity wave in this Mach number range the wavelength of the transmitted vorticity wave is only one-third that for the generated acoustic wave. For $\lambda = 1$ at Mach 2 there are only 9 grid points per wavelength (in the x-direction) for the transmitted vorticity wave. This wave is not adequately resolved under these circumstances. For $\lambda = 2$, however, the generated acoustic wave is so long (it has a wavelength in the x-direction of 2.7) that a full wavelength has not yet established itself behind the shock. Perhaps the discrepancy here is due to transient effects.

An interesting observation about these nonlinear calculations is that by tailoring the wavelength of a low amplitude incident wave to suit a specific response wave, the linear theory prediction for that particular response can be reproduced well. This occurs despite what may be a poor environment for the other response waves. This suggests that the numerical scheme permits low amplitude waves to propagate independently behind the shock. The shock-fitting aspects of the numerical algorithm have the very high resolution at the shock front which is required for the crucial task of calculating the amplification and generation of waves.

Conclusions

The numerical results of the previous section confirm the validity of the linear theory of the interactions of plane waves with shocks in two of its three questionable regimes - weak shocks and strong disturbances. The linear theory remains reliable to extraordinarily large amplitudes. In some of the examples the post-shock velocity fluctuations were of nearly the same order as the mean stream velocity.

On the other hand there is a serious discrepancy between the numerical results and the linear predictions for the remaining questionable regime - waves with incidence angles near or beyond the critical angle. Perhaps it takes much longer for the initial transients to settle down whenever the acoustic response is evanescent. Even if this proves to be the reason for the disagreement, it will still point to a deficiency in applying the linear theory to real turbulence, which after all consists of transient phenomena and not steady plane waves

Much work remains to be done on the shock wave-turbulent boundary layer interaction problem. In a subsequent paper we will report on numerical calculations of shock interactions with coherent, transient vorticity and entropy fluctuations as well as calculations pertaining to the focusing and shock oscillation mechanisms. Of course, this work must eventually be extended to three dimensions so that vortex stretching is permitted.

REFERENCES

[1]Bushnell, D. M., Cary, A. M., Jr., and Harris, J. E., "Calculation Methods for Compressible Turbulent Boundary Layers," NASA SP-422, 1976.

[2]Viegas, J. R. and Horstman, C. C., "Comparison of Multi-Equation Turbulence Models for Several Shock Separated Boundary-Layer Interaction Flows," AIAA Journal, Vol. 17, No. 8, August 1979, pp. 811-820.

[3]Horstman, C. C., Hung, C. M., Settles, G. S., Vas, I. E., and Bogdonoff, S. M., "Reynolds Number Effects on Shock-Wave/Turbulent Boundary-Layer Interactions — A Comparison of Numerical and Experimental Results," AIAA Paper 77-42, 1977.

[4]Deissler, R. G., "Evolution of a Moderately Short Turbulent Boundary Layer in a Severe Pressure Gradient," Journal of Fluid Mechanics, Vol. 64, Part 4 July 1974, pp. 763-774.

[5]Narasimha, R. and Prabhu, A., "Equilibrium and Relaxation in Turbulent Wakes," Journal of Fluid Mechanics, Vol. 54, Part 1, July 1972, pp. 1-17.

[6]Rose, W. C., "The Behavior of a Compressible Turbulent Boundary Layer in a Shock-Wave-Induced Adverse Pressure Gradient," NASA TN D-7092, 1973.

[7]Mateer, G. C., Brosh, A., and Viegas, J. R., "A Normal Shock-Wave Turbulent Boundary-Layer Interaction at Transonic Speeds," AIAA Paper 76-161, 1976.

[8]Sekundoz, A. N., "Supersonic Flow Turbulence and Its Interaction with a Shock Wave," Akademiia Nauk SSSR, Izvestiia, Mekhanika Zhidkosti i Gaza, No. 2, March-April 1974, pp. 8-16.

[9]Delery, J. M., "Experimental Investigation of Turbulence Properties in Transonic Shock/Boundary-Layer Interactions, AIAA Journal, Vol. 21, No. 2, February 1983, pp. 180-185.

[10]Marenbach, G., "Experimental Investigation of the Interaction Between a Turbulent Sonic Wake and a Compression Shock," Paper 81-022, Deutsche Gesellschaft für Luft-und Raumfahrt, Jahrestagung, Aachen, West Germany, May 11-14, 1981.

[11]Hayakawa, K., Smits, A. J., and Bogdonoff, S. M., "Hot Wire Investigation of an Unseparated Shock-Wave/Turbulent Boundary Layer Interaction," AIAA Paper 82-0985, 1982.

[12]Gol'dfel'd, M. A. and Zatoloka, V. V., "On the Improvement of Separating Properties of a Turbulent Boundary Layer as a Result of the Effect of a Shock Wave," Akademiia Nauk SSSR, Sibirskoe Otdelenie Izvestiia, No. 3, October 1979, pp. 40-47.

[13]Kovasnay, L. S. G., "Turbulence in Supersonic Flow," Journal of the Aeronautical Sciences, Vol. 20, No. 10, October 1953, pp. 657-674.

[14]Moore, F. K., "Unsteady Oblique Interaction of a Shock Wave with a Plane Disturbance," NACA Report 1165, 1954.

[15]Ribner, H. S., "Shock-Turbulence Interaction and the Generation of Noise," NACA Report 1233, 1955.

[16]Chang, C. T., "On the Interaction of Weak Disturbances and a Plane Shock of Arbitrary Strength in a Perfect Gas," Ph.D. Thesis, The Johns Hopkins University, 1955.

[17]Kerrebrock, J. L., "The Interaction of Flow Discontinuities with Small Disturbances in a Compressible Fluid," Ph.D. Thesis, California Institute of Technology, 1956.

[18]Ribner, H. S. and Moore, F. K., "Unsteady Interaction of Disturbances with a Shock Wave with Applications to Turbulence and Noise," Proceedings, 1953 Heat Transfer and Fluid Mechanics Institute, pp. 45-55.

[19]Chang, C. T., "Interaction of a Plane Shock and Oblique Plane Disturbances with Special Reference to Entropy Waves," Journal of the Aeronautical Sciences, Vol. 24, No. 9, September 1957, pp. 675-682.

[20]Morkovin, M. V., "Note on the Assessment of Flow Disturbances at a Blunt Body Traveling at Supersonic Speeds Owing to Flow Disturbances in Free Stream," Journal of Applied Mechanics, Vol. 27, No. 2, June 1960, pp. 223-229.

[21]Cuadra, E., "Interactions of a Shock Wave with an Entropy Discontinuity," Wyle Laboratories Report No. WR 67-17, 1968.

[22]Cuadra, E., "Flow Perturbations Generated by a Shock Wave Interacting with an Entropy Wave," AFOSR-UTIAS Symposium on Aerodynamic Noise, Toronto, May 20-21, 1968, pp. 251-271.

[23]Anyiwo, J. C. and Bushnell, D. M., "Turbulence Amplification in Shock Wave Boundary Layer Interactions," AIAA Journal, Vol. 20, No. 7, July 1982, pp. 893-899.

[24]Pierce, A. D., "Spikes on Sonic-Boom Pressure Waveforms," Journal of the Acoustical Society of America, Vol. 44, No. 4, October 1968, pp. 1052-1061.

[25]Sturtevant, B. and Kulkarny, V. A., "The Focusing of Weak Shock Waves," Journal of Fluid Mechanics, Vol. 73, Part 4, February 1976, pp. 651-671.

[26]Johnson, D. A., Horstman, C. C., and Bachalo, W. D., "A Comprehensive Comparison Between Experiment and Prediction for a Transonic Turbulent Separated Flow," AIAA Paper 80-1407, 1980.

[27]Vidal, R. J., Wittliff, C. E., Catlin, P. A., and Sheen, B. H., "Reynolds Number Effects on the Shock Wave - Turbulent Boundary Layer Interaction at Transonic Speeds," AIAA Paper 73-661, 1973.

[28]Grande, E. and Oates, G. C., "Unsteady Flow Generated by Shock-Turbulent Boundary Layer Interactions," AIAA Paper 73-168, 1973.

[29]Raghunathan, S., Coll, J. B., and Mabey, D. G., "Transonic Shock/Boundary Layer Interaction Subject to Large Pressure Fluctuations," AIAA Journal, Vol. 17, No. 12, December 1979, pp. 1404-1406.

[30]Henderson, L. F., "The Reflexion of a Shock Wave at a Rigid Wall in the Presence of a Boundary Layer," Journal of Fluid Mechanics, Vol. 30, Part 4, December 1967, pp. 699-722.

[31]MacCormack, R. W., "Numerical Solution of the Interaction of a Shock Wave with a Laminar Boundary Layer," Lecture Notes in Physics, Vol. 8, Springer-Verlag, New York, 1971, p. 151.

[32]Pao, S. P. and Salas, M. D., "A Numerical Study of Two-Dimensional Shock Vortex Interaction," AIAA Paper 81-1205, 1981.

[33]Hussaini, M. Y., Salas, M. D., and Zang, T. A., "Spectral Methods for Inviscid Compressible Flows," in Advances in Computational Transonics, W. G. Habashi, ed., Pineridge Press, Swansea, U.K., 1983.

[34]McKenzie, J. F. and Westphal, K. O., "Interaction of Linear Waves with Oblique Shock Waves," Physics of Fluids, Vol. 11, No. 11, November 1968, pp. 2350-2362.

[35]Zang, T. A., Kopriva, D. A., and Hussaini, M. Y., "Pseudospectral Calculations of Shock-Turbulence Interactions," presented at the International Conference on Numerical Methods in Laminar and Turbulent Flow, August 8-11, 1983, Seattle, WA.

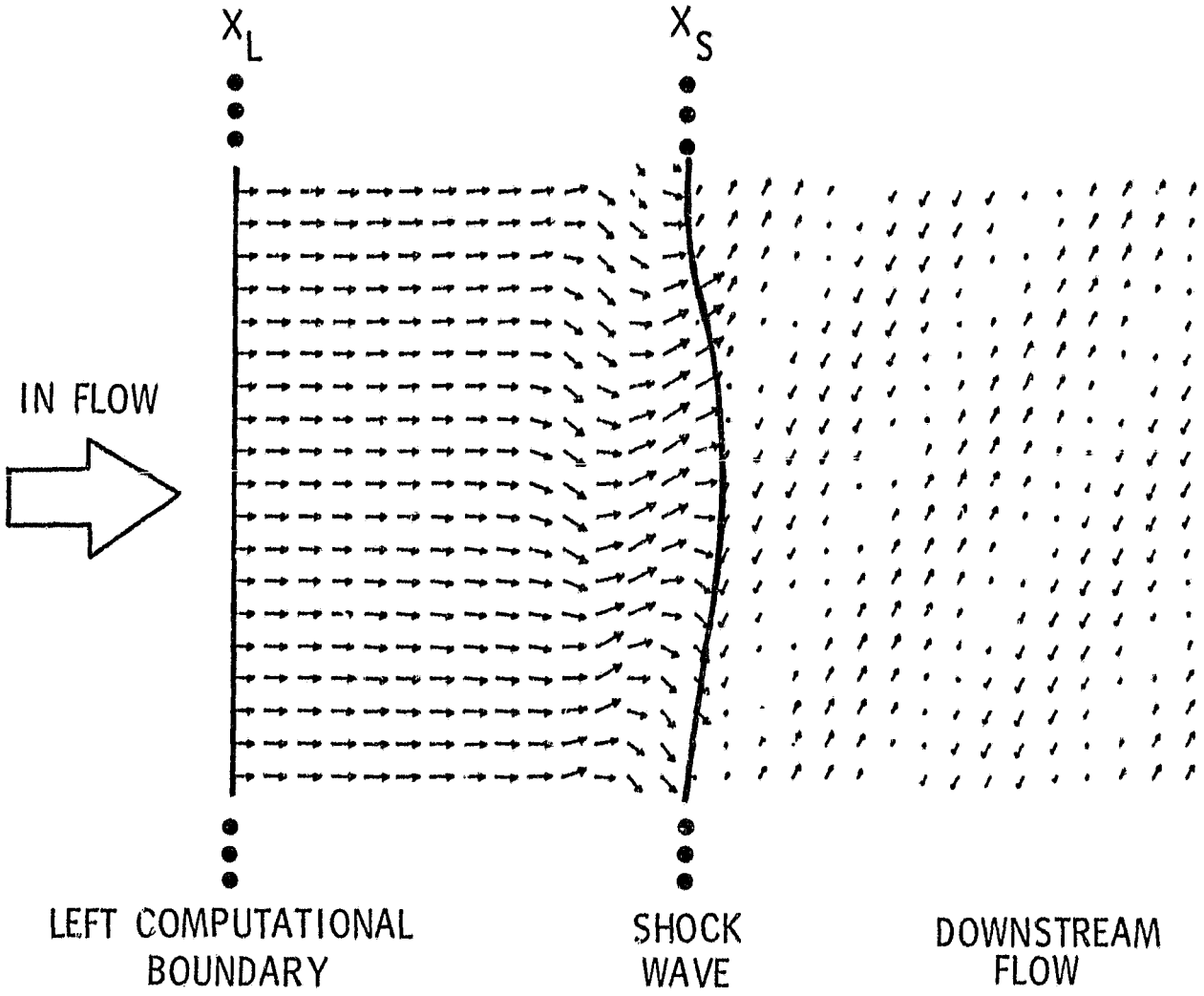

Fig. 1. Model problem in the physical domain.

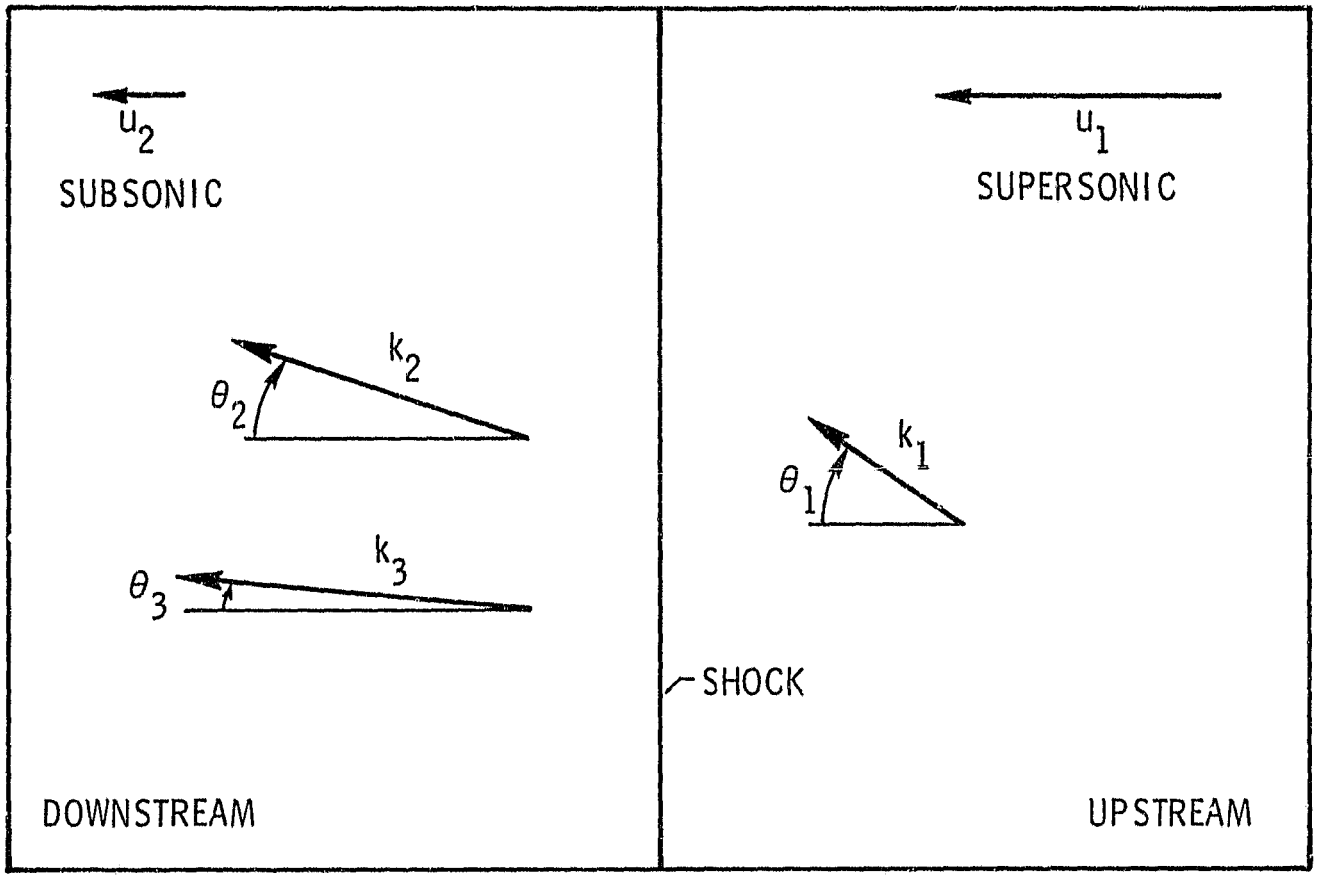

Fig. 2. Refracted acoustic ($\underline{k}_2$) and entropy-vorticity ($\underline{k}_3$) wavevectors for an acoustic wave ($\underline{k}_1$) with an incidence (θ_1) of 30° to a Mach 8 normal shock. The refracted entropy-vorticity wavevector is drawn to 1/3 the scale of the others. In this illustration the shock is stationary, which is a convenient frame for linear theory.

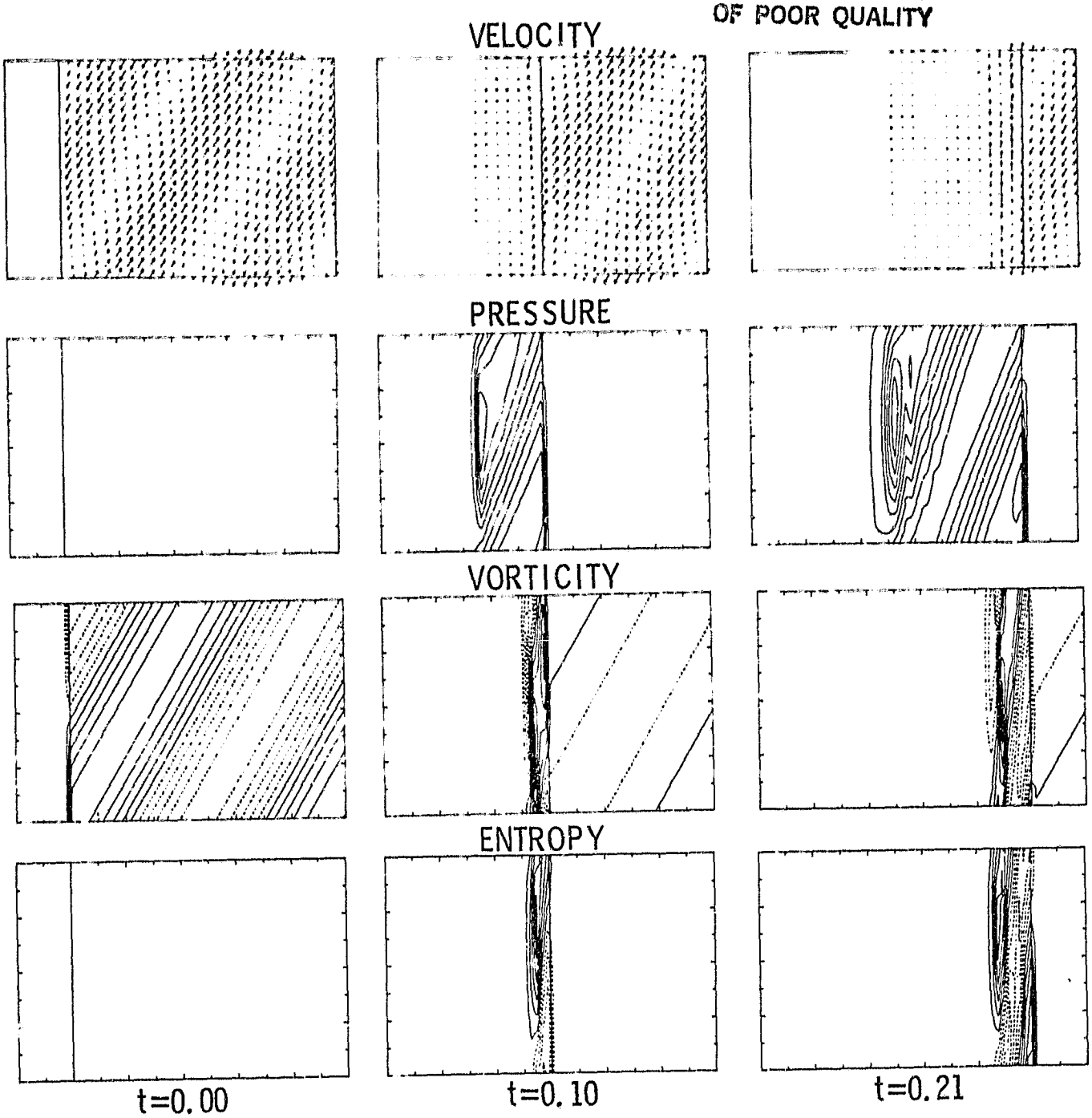

Fig. 3 Evolution in the computational frame of a 1% vorticity wave striking a Mach 8 shock at a 30^{o} angle of incidence. The shock front is denoted by the solid line connecting the top and bottom boundaries. Separate scales are chosen in each frame for the velocity vectors and contour lines. The velocity vectors represent the perturbations from the initial mean flow. Dashed lines indicate negative contour levels. The plotting domain extends from -0.5 to 2.5 in x and from -1 to +1 in y.

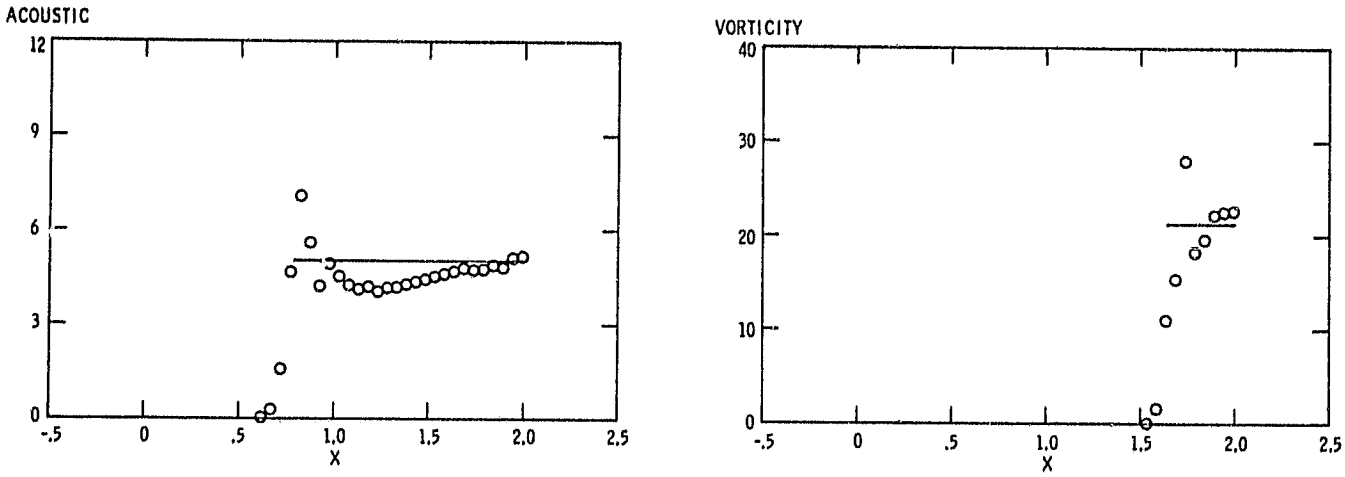

Fig. 4. Upstream dependence at time $t = 0.21$ of the acoustic (left) and vorticity (right) responses to a 0.1% vorticity wave incident at 30° to a Mach 8 shock. The solid lines are the linear theory predictions. The computed responses are given in the MW units.

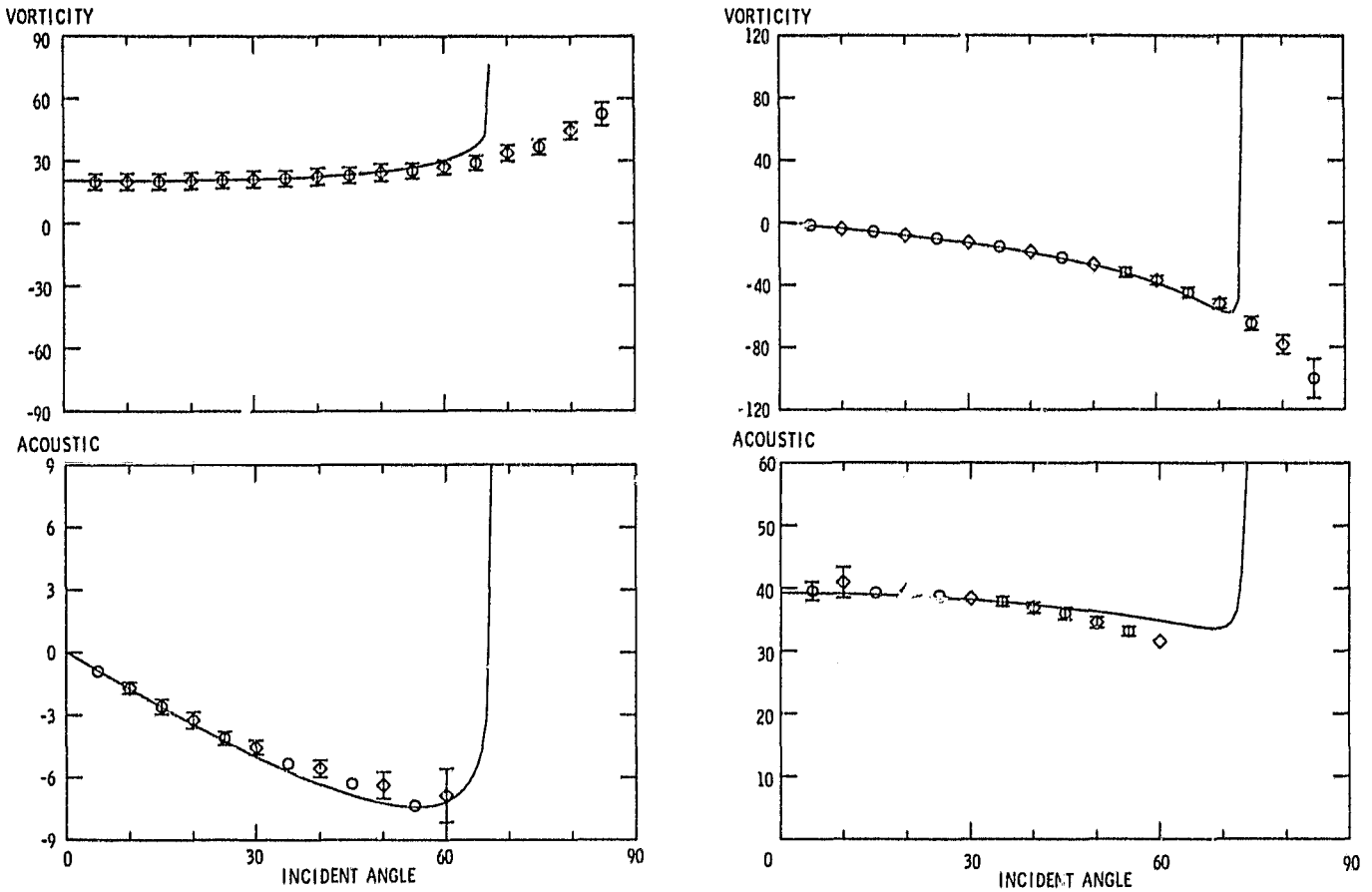

Fig. 5. Incident angle dependence of the vorticity (top) and acoustic (bottom) responses to waves incident upon a Mach 8 shock. Responses to incident vorticity waves are shown in the left column; responses to incident acoustic waves are on the right. The solid lines are the linear theory predictions below the critical angle. The computed responses to both 0.1% (circles) and 10% (diamonds) incident waves are given in the MW units.

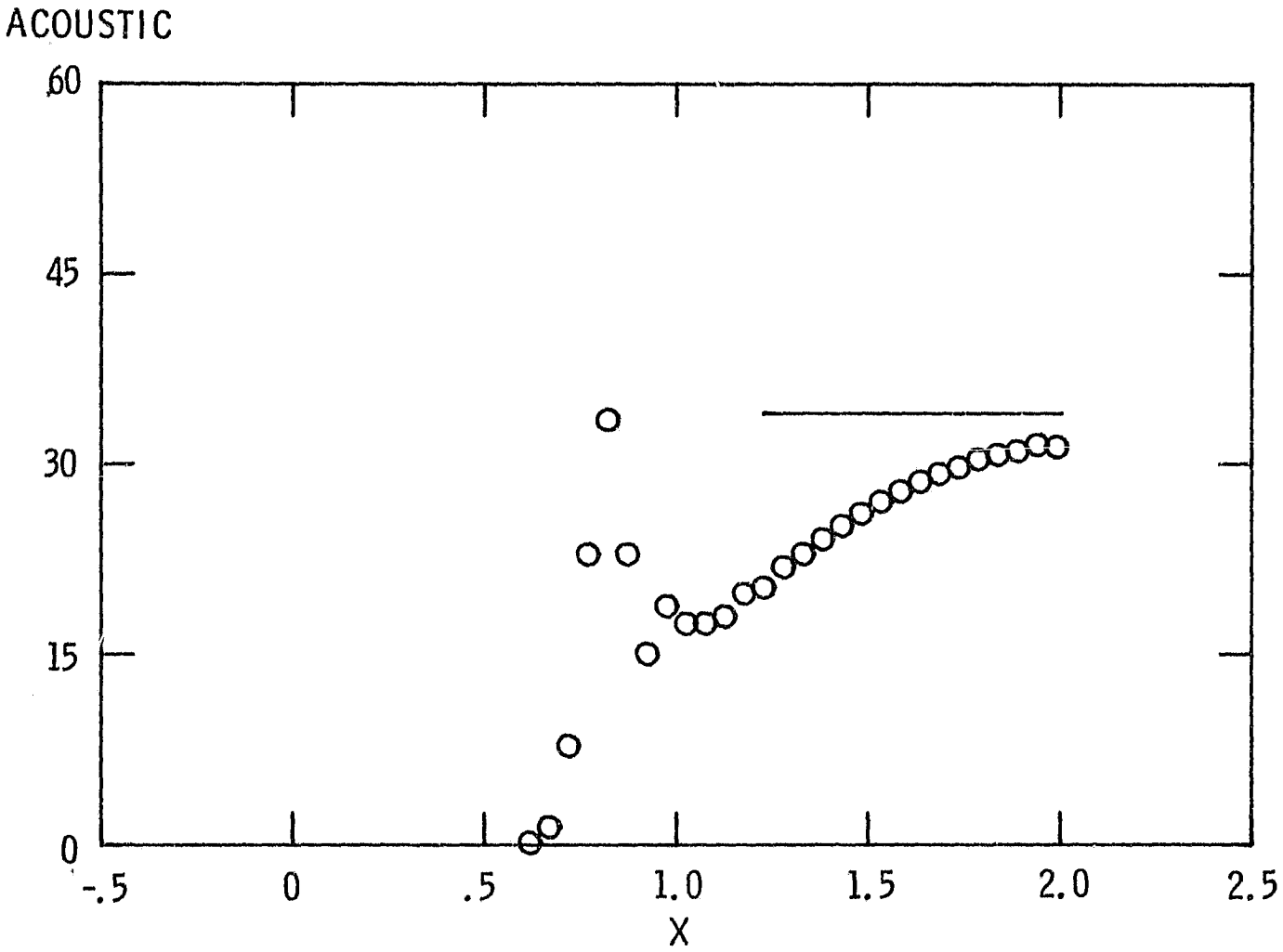

Fig. 6. Upstream dependence at time 0.21 of the acoustic response to a 0.1% vorticity wave incident at 65° to a Mach 8 shock. The solid line is the linear theory prediction. The computed responses are given in the MW units.

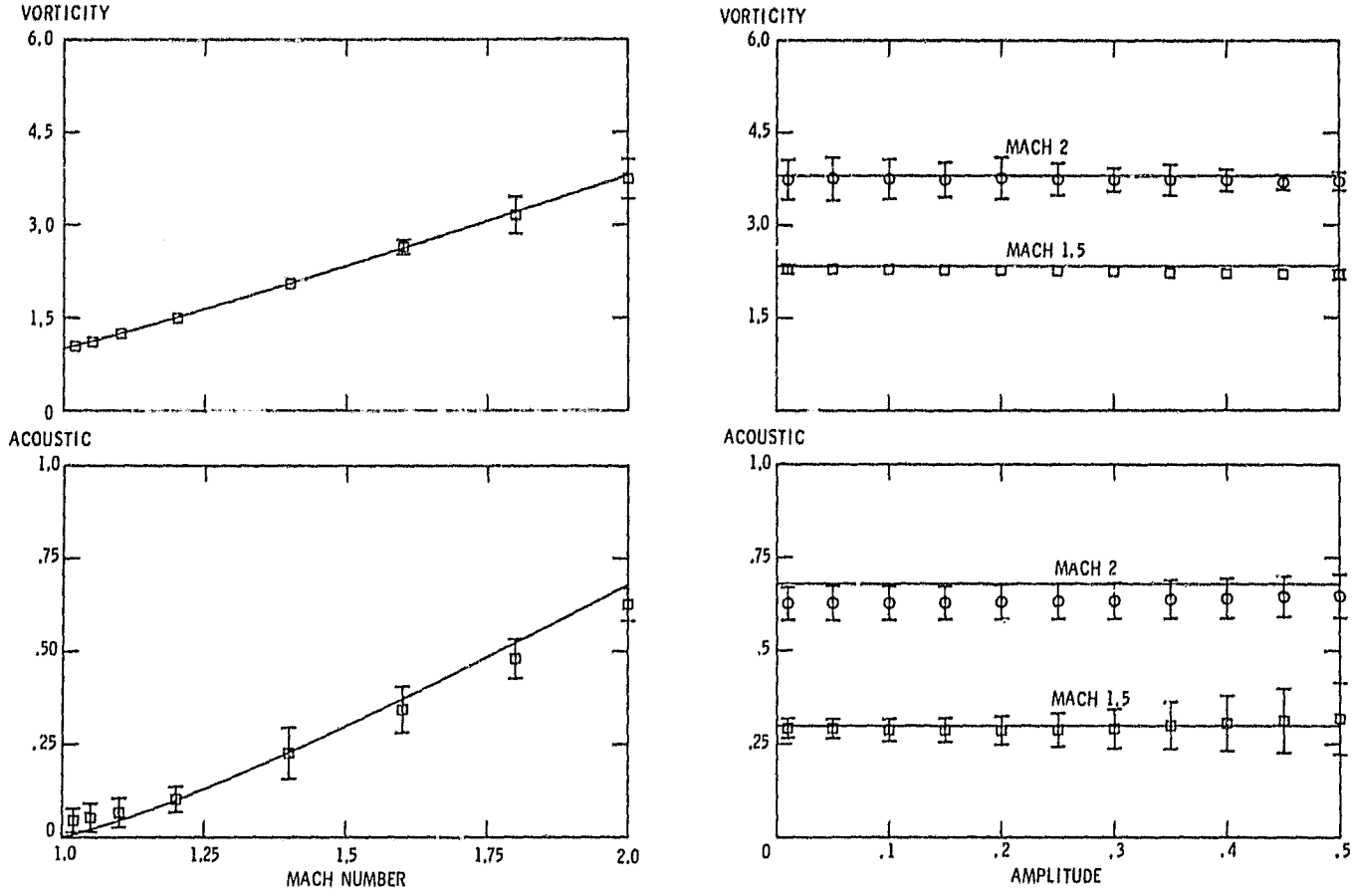

Fig. 7. Mach number and amplitude dependence of vorticity (top) and acoustic (bottom) responses to vorticity waves at 30° incidence. The Mach number results shown by the squares in the left column were obtained for 1% incident waves. The amplitude dependence shown in the right column was computed for Mach 2 (circles) and Mach 1.5 (squares) shocks. The solid lines are the linear theory predictions.

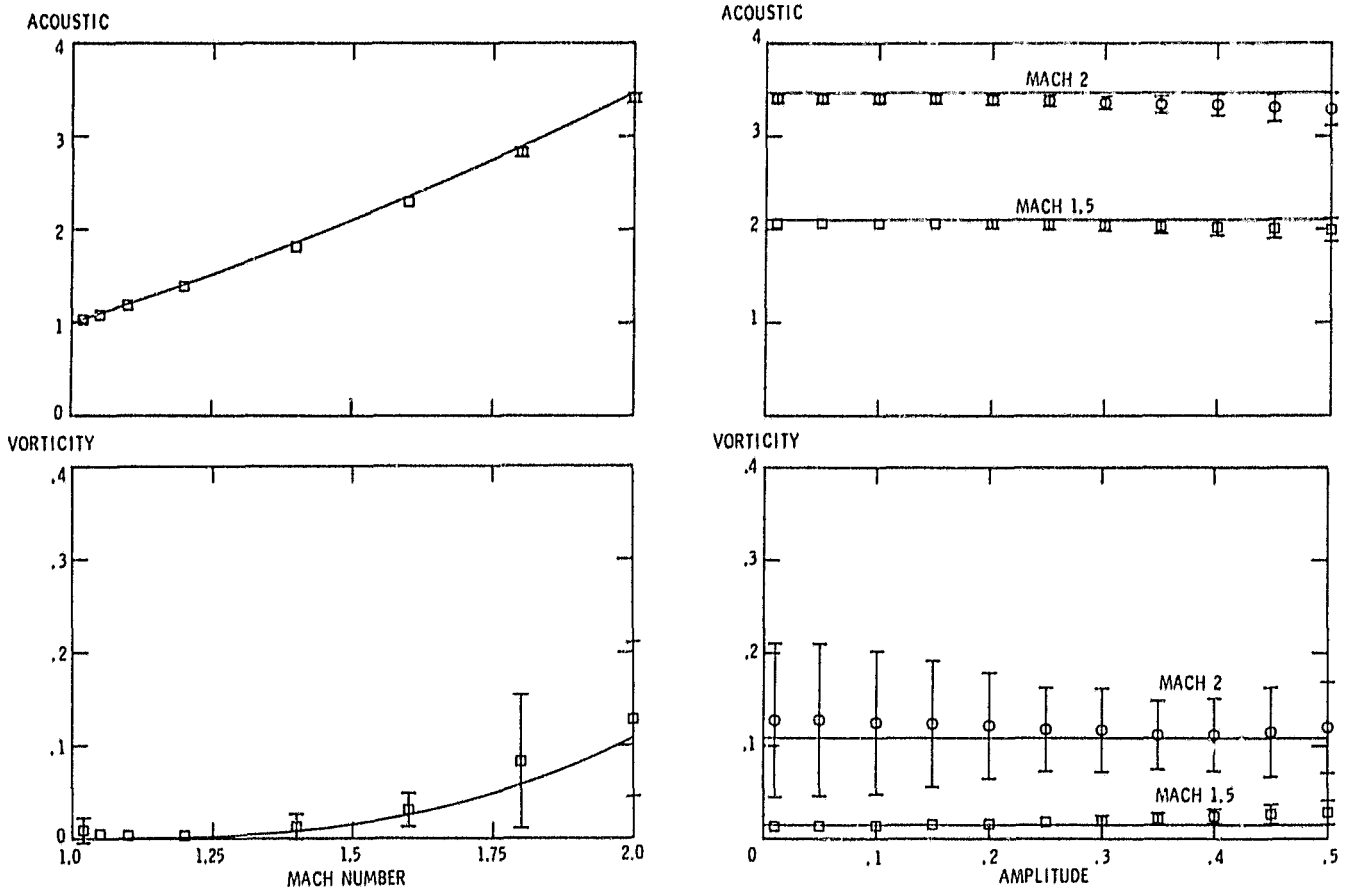

Fig. 8. Mach number and amplitude dependence of acoustic (top) and vorticity (bottom) responses to acoustic waves at 30° incidence. The Mach number results shown by the squares in the left column were obtained for 1% incident waves. The amplitude dependence shown in the right column was computed for Mach 2 (circles) and Mach 1.5 (squares) shocks. The solid lines are the linear theory predictions.

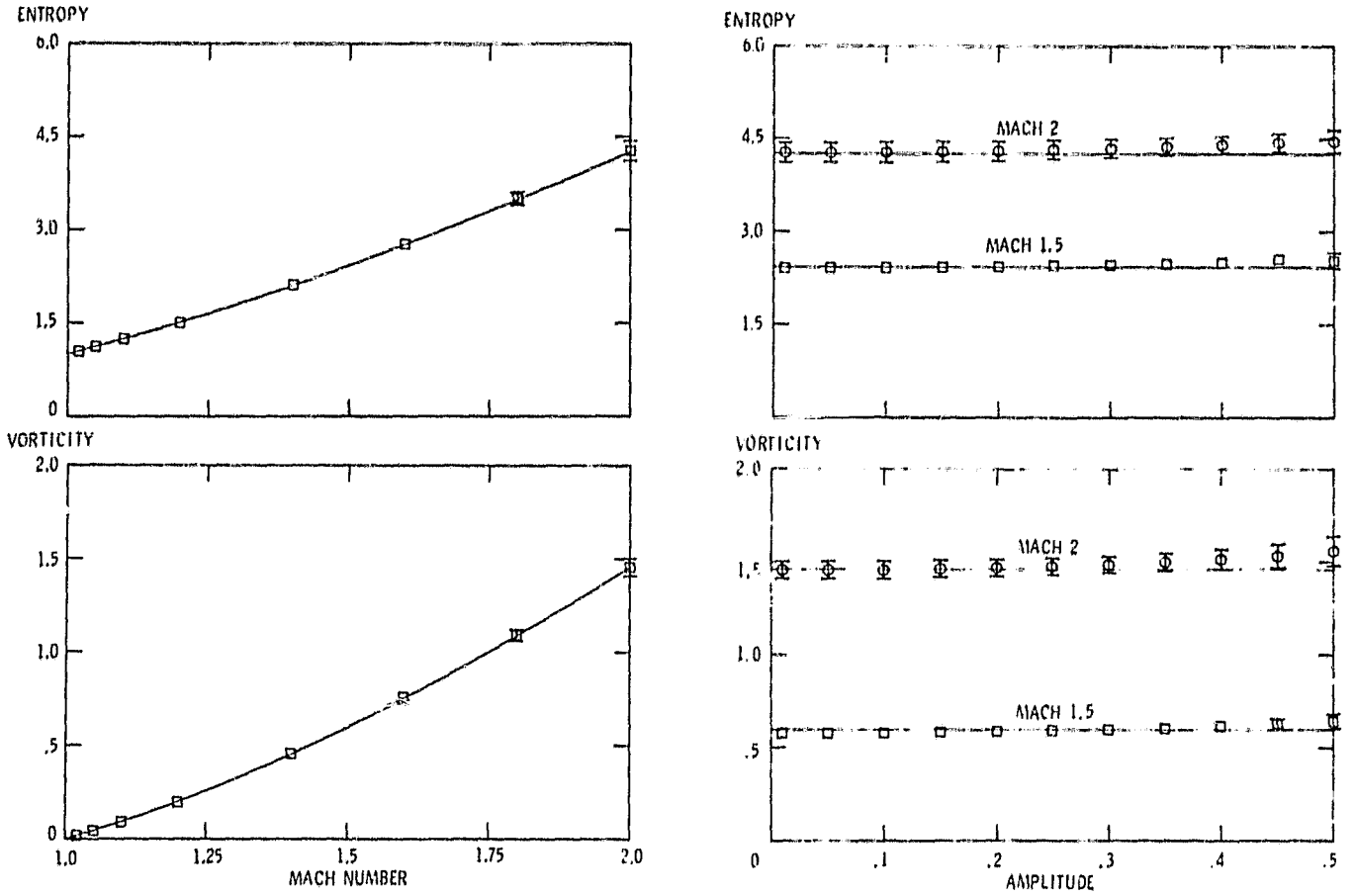

Fig. 9. Mach number and amplitude dependence of entropy (top) and vorticity (bottom) responses to entropy waves at 30° incidence. The Mach number results shown by the squares in the left column were obtained for 1% incident waves. The amplitude dependence shown in the right column was computed for Mach 2 (circles) and Mach 1.5 (squares) shocks. The solid lines are the linear theory predictions.